Food Chemistry: X 20 (2023) 100995

Contents lists available at ScienceDirect

Food Chemistry: X

journal homepage: www.sciencedirect.com/journal/food-chemistry-x

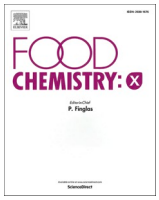

Development of composite electrospun films utilizing soy protein amyloid fibrils and pullulan for food packaging applications

Yabo Dong [a], Tian Lan [a], Luying Wang [a], Xing Wang [a], Zejian Xu [a], Lianzhou Jiang [a], Yan Zhang [b], Xiaonan Sui [a,*]

[a] College of Food Science, Northeast Agricultural University, Harbin 150030, China
[b] College of Horticulture and Landscape Architecture, Northeast Agricultural University, Harbin 150030, China

ARTICLE INFO

Keywords:
Electrospun nanofibers
Orally disintegrating films
Pullulan
Soy protein amyloid fibrils

ABSTRACT

Electrospun films (ESF) are gaining attention for active delivery due to their biocompatibility and biodegradability. This study investigated the impact of adding soy protein amyloid fibrils (SAFs) to ESF. Functional ESF based on SAFs/pullulan were successfully fabricated, with SAFs clearly observed entangled in the electrospun fibers using fluorescence microscopy. The addition of SAFs improved the mechanical strength of the ESF threefold and increased its surface hydrophobicity from 24.8° to 49.9°. Moreover, the ESF demonstrated antibacterial properties against *Escherichia coli* and *Staphylococcus aureus*. In simulated oral disintegration tests, almost 100% of epigallocatechin gallate (EGCG) dissolved within 4 min from the ESF. In summary, the incorporation of SAFs into ESF improved their mechanical strength, hydrophobicity, and enabled them to exhibit antibacterial properties, making them promising candidates for active delivery applications in food systems. Additionally, the ESF showed efficient release of EGCG, indicating their potential for controlled release of bioactive compounds.

1. Introduction

Electrospun is a mild, efficient, and scalable processing method that allows for the fabrication of continuous nanofibers with diameters in the micron and nanometer range using biopolymers in aqueous solutions once they surpass the critical voltage (Dos Santos et al., 2020). Therefore, films prepared by electrospun offer numerous advantages such as high porosity, high surface area, and ultrafine and oriented structure. Electrospun films (ESF) are commonly utilized in the food industry for food active packaging and the delivery of bioactive components. As a novel delivery system, ESF offers various benefits, such as high encapsulation efficiency and multifunctionality (Peng et al., 2017). To ensure suitability for different usage environments, the selection of electrospun materials is crucial for preparing ESF films with diverse properties. Natural polymers like polysaccharides and proteins are popular due to their non-toxic, biodegradable, and biocompatibility. However, ESF prepared from single components typically exhibit drawbacks such as low strength, limited hydrophobicity, and reduced functionality (Niu et al., 2020). In recent years, multi-component blends consisting of materials like gelatin, starch, chitosan, cinnamaldehyde, carrageenan and cellulose have been increasingly employed to enhance the properties of ESF.

SAFs are considered a promising approach to enhance and diversify protein functionalities due to their ordered structure and extreme aspect ratios (Peydayesh & Mezzenga, 2021). The use of SAFs as delivery carriers in the food and medical fields holds great promise due to their multiple functional groups, which can facilitate different interactions with various nutrients and drugs (Tang, 2019). Recent applications of SAFs include using whey protein isolate fibrils as carriers for iron fortification, resulting in delayed iron release (Yue et al., 2022). Hen egg lysozyme was used to stabilize high internal phase emulsions for encapsulation and protection of lutein (Leng et al., 2022). Protein amyloid fibrils have also been used in film preparation. Hybrid films prepared from plasticizers and amyloid protofibrils (lysozyme or β-lactoglobulin fibrils) showed extremely high elastic moduli (5.2–7.2 GPa) (Knowles, Oppenheim, Buell, Chirgadze, & Welland, 2010). Considering the edible applications of these prepared films, soy protein stands out for its balanced amino acid profile compared to other proteins. Moreover, it is more readily available and processed than many other plant-derived proteins and animal protein-derived foods.

* Corresponding author.
E-mail address: xiaonan.sui@neau.edu.cn (X. Sui).

https://doi.org/10.1016/j.fochx.2023.100995
Received 28 July 2023; Received in revised form 28 October 2023; Accepted 8 November 2023
Available online 11 November 2023

Therefore, the application of SAFs presents great potential than other material sources. In addition, there have been limited studies on electrospun using SAFs and even fewer related applications.

Pullulan consists of α-(1 → 6) linked maltotriose units and is a non-toxic, odorless, tasteless and edible water-soluble microbial polysaccharide (Drosou, Krokida, & Biliaderis, 2022). Pullulan has unique film- and fiber-forming properties due to its unique linkage pattern. Many studies have reported the use of pullulan in the preparation of ESF. However, films prepared from pullulan alone often lack optimal performance. To meet the requirements of various usage environments, it's essential to carefully select electrospun materials for preparing ESF with different properties. While composite films can enhance certain properties of films, such as hydrophobicity, antimicrobial activity, and mechanical strength, achieving multiple property enhancements with a single compound can be challenging.

Epigallocatechin-3-gallate (EGCG), the most abundant catechin in green tea, is the most effective tea polyphenol in trapping reactive oxygen species. In addition to its high radical scavenging properties, EGCG has attracted interest for potential medical applications, such as possible antiviral, antibacterial, and neuroprotective activity. It also exhibits other functionalities, such as its ability to interact with proteins to improve functionality and its capacity to coordination with catechol structures and metal ions to form metal-polyphenol networks for the production of various functional materials (Dong et al., 2021).

In this study, soy protein amyloid fibrils were used for the first time in the process of electrospun. SAFs were mixed with pullulan to create hybrid electrospun films with enhanced functionality. The effect of adding SAFs on the morphology of ESF was investigated by scanning electron microscopy and fluorescence microscopy. Furthermore, the structural changes, antibacterial properties, mechanical strength and water absorption properties of the ESF were systematically analyzed. Additionally, oral epigallocatechin gallate (EGCG) has been reported to have therapeutic effects for specific diseases, such as colitis (Mehmood et al., 2022). Therefore, this study explored the potential application of ESF as an oral rapid release film for EGCG delivery.

2. Materials and methods

2.1. Materials

Pullulan (MW ≈ 200 kDa) was purchased from Peiyang biotrans Biotechnology Co., Ltd. (Tianjin, China). Soybeans were purchased from a High-Tech company (Harbin, Heilongjiang, China). EGCG from green tea (purity ≥ 98 %) and Thioflavin T (ThT) (purity ≥ 75 %) were purchased from Yuanye Biotechnology Co., Ltd (Shanghai, China). All reagents were used without further purification. Deionized (DI) water was used throughout the study.

2.2. Preparation of soy protein amyloid fibrils

Preparation of soy protein isolate (SPI) and SAFs were performed according to our previous study (Dong et al., 2020; Xu et al., 2022). SPI was dissolved in DI water at pH 2 (with 6 mol/L HCl). The resulting protein solution was centrifuged to remove any insoluble material. The protein concentration in the final solution was 3.0 % (w/w). Next, the solution was heated in an oil bath at 85 °C for 20 h with stirring (100 rpm) to obtain SAFs.

2.3. Characterization of soy protein amyloid fibrils

2.3.1. Fibrils concentration

The fibrils concentration of SAFs (the amount of protein converted into fibrils) was measured according to Akkermans et al. (2007). The diluted SAFs solution (2 mL) was filtered using centrifugal filter units (Amicon Ultra 100 K-15 centrifugal filters, Millipore, MA, USA) at 1000 × g for 30 min at 4 °C. The residual protein was washed with DI water at pH 2.0 and this step was repeated until there is no residual protein in the last filtrate. The amount of converted protein was determined from the amount of protein present in the retentate using Lowry's method. The difference between the total amount of additional protein and protein unconverted to fibrils was used as the amount of protein converted into fibrils.

2.3.2. Thioflavin T fluorescence

A Thioflavin T solution (18 mg/L) was prepared by dissolving ThT in a phosphate buffer (pH 7.0) containing 150 mM NaCl. The undissolved ThT was removed with a syringe filter. SAFs solution (50 μL) was mixed thoroughly with 10 mL of ThT solution. Measurement of fluorescence spectra of mixtures with RF-6000 spectrofluorometer (Shimadzu Corporation, Kyoto, Kyoto Prefecture, Japan). The excitation wavelength was 460 nm with slit widths of 10 nm, and the emission of the sample was measured from 450 to 600 nm (scanning speed = 900 nm/min).

2.3.3. Atomic force microscopy

The diluted SAFs solution (0.01 g/L, 50 μL) was dopped on a fleshly cleaved mica surface and dried at room temperature for 12 h. The mica sheets were about 1.0 × 1.0 cm^2. AFM images of SAFs were recorded using a Bruker Dimension Fast Scan microscope in tapping mode (Bruker Corp., Karlsruhe, Germany). The AFM images were analyzed using Nanoscope analysis 1.5 software (Bruker, Germany).

2.4. Electrospun process

The pH of the pullulan solution (30 %, w/v) was adjusted to 2.0 using HCl (2 mol/L). The electrospun solutions were prepared by mixing 30 % (w/v) pullulan solution with the SAFs or SPI at mass ratios of 10:0, 9:1, 8:2,7:3 and 6:4 (PUL, SAFs/PUL 1:9, SAFs/PUL 2:8, SAFs/PUL 3:7, SAFs/PUL 4:6, SPI/PUL 4:6, respectively). The electrospun solutions were stirred (100 rpm) for 2 h at room temperature to fully mix the pullulan and SAFs. The pH was monitored and adjusted to 2.0. Next, electrospun solutions were drawn in a syringe with a 20 G steel needle for electrospun. The electrospun parameters were as follows: the flow rate is 0.5 mL/h, the voltage is 15 kV, the wire with the voltage is bound to the needle of the syringe by a copper wire and the tip-collector distance is 15 cm. The relative humidity and temperature were maintained at approximately 50 % RH and room temperature (25 °C), respectively.

2.5. Characterization of solution properties

The conductivity was recorded by a DDSJ-318 conductometer (Leici, Shanghai, China). The viscosity of the mixture solutions was measured using an NDJ-9S rotary viscometer (Lichen, Shanghai, China) equipped with No. 2 rotor. The surface tension was measured by a Theta contact angle goniometer (Biolin Scientific, Goteborg, Sweden). All measurements were performed in triplicate at 25 °C.

2.6. Scanning electron microscopy

The scanning electron microscopy (SEM) images experiment was conducted according to the method of Xu et al. (2022) using a Hitachi S-3400 N SEM system (Hitachi, Japan). Aluminum foil with electrospun fibers was cut into small rectangular pieces and sprayed with gold powder. Images were recorded at 5 kV and a magnification of 2000 × under a high vacuum. The fiber diameters were determined using Image J software (version 1.51n; National Institutes of Health, USA).

2.7. Fluorescence microscopy

The distribution of the SAFs in the electrospun fiber was investigated using a fluorescence microscope (DMI8, Leica, Wetzlar, Germany). The SAFs solution was stained using ThT. According to the previous step, the stained SAFs solution was mixed with the pullulan solution. The

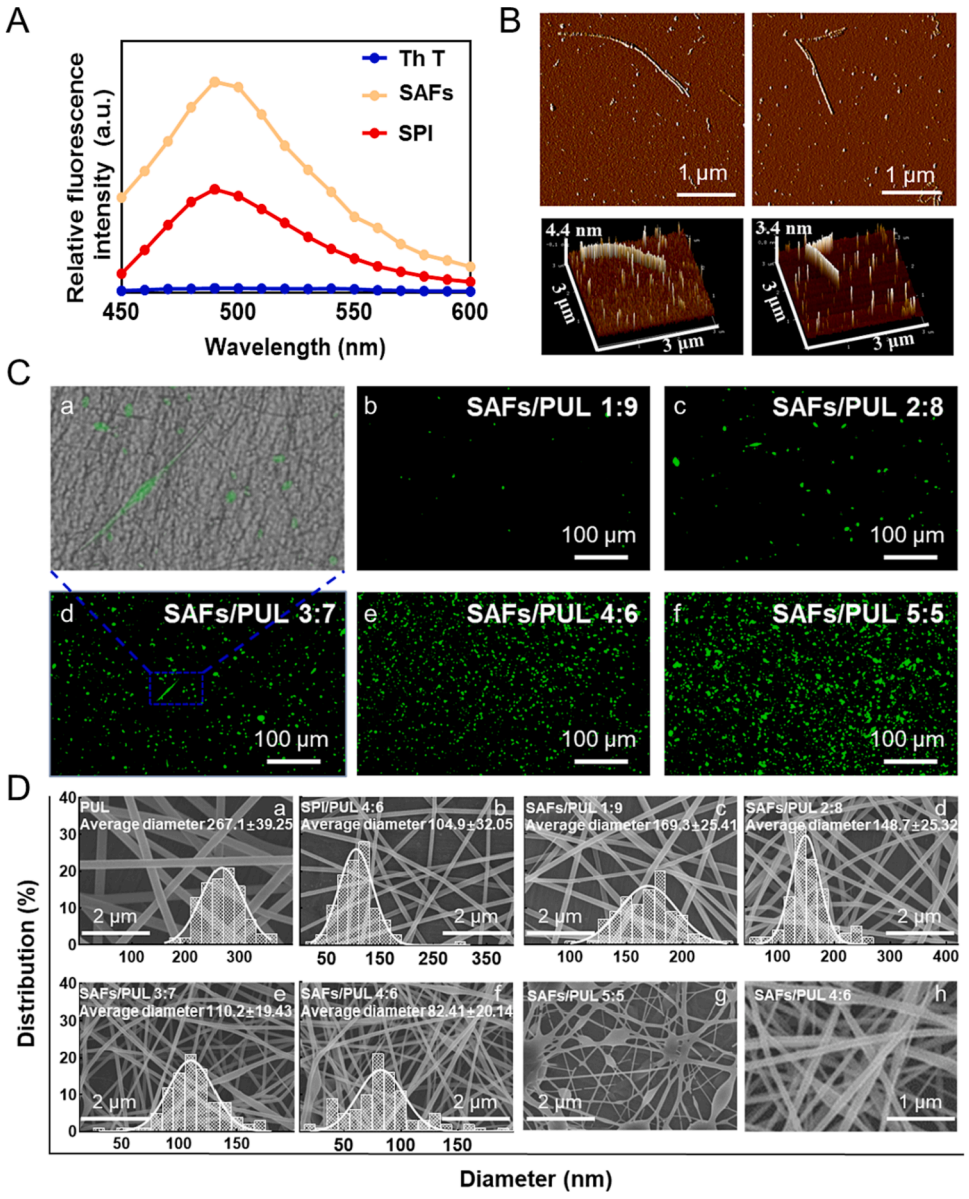

Fig. 1. (A) ThT fluorescence intensity of SAFs and SPI. (B) Morphology examination of SAFs using AFM. (C) Fluorescence microscopy images of SAFs/PUL ESF at the ratio of 1:9; 2:8; 3:7; 4:6 and 5:5. (D) SEM images of PUL ESF; SAFs/PUL ESF and SPI/PUL ESF.

electrospun fibers were collected using slides under lightproof conditions.

2.8. Fourier transform infrared spectroscopy

Fourier transform infrared (FTIR) spectra were recorded using a Magna 750 spectrometer (Nicolet, Madison, USA) according to our previous study (Dong et al., 2021). The fabricated samples (SPI, SAFs, PUL, and ESF) were compressed with KBr at 1:100 (w/w) and recorded in the wavenumber range 500–4000 cm^{-1} at a resolution of 4 cm^{-1} with 32 scans. The quantitative analysis of the secondary structure of the protein using PeakFit software (4.12, SeaSolve Software, Richmond, USA).

2.9. X-ray diffraction

The characteristic diffraction patterns of samples (SPI, SAFs, PUL, and ESF) were measured with X-ray diffraction (XRD) (Malvern Panalytical, Almelo, Netherlands) according to the report of Xu et al. (2019). The Cu-Kα radiation (λ = 1.5418 Å) was generated at 60 mA with a voltage of 40 kV. Measurement was taken in the scattering range of (2θ) from 5° to 45° (scanning rate; 2°/min, step size; 0.02°).

2.10. Water contact angle

The water contact angle (WCA) was measured according to the method of (Yang, Xie, Liu, Kong, & Wang, 2020) using the Theta contact angle goniometer (Biolin Scientific, Goteborg, Sweden) at room temperature (25 °C). The WCA was obtained by dropping 5 μL water onto the surface of the ESF and equilibrated for 1 s.

2.11. Moisture sorption isotherms

Dried film samples (approximately 800 mg) were placed in previously weighed Petri dishes and kept in closed desiccators over saturated salt solutions at three different temperatures (25 °C, 35 °C and 45 °C) for 21 days. The various relative humidity conditions in the closed sample bottles were reached by the following salt solutions: CH_3COOK, K_2CO_3,

$NaNO_2$, KCl and KNO_3 which give A_w values (25 °C) of 0.23, 0.43, 0.64, 0.84 and 0.94, respectively (Fabra, Talens, & Chiralt, 2010). After reaching equilibrium moisture, the ESF moisture content was determined using the weighing method. The A_w-moisture data were fitted to the Brunauer–Emmett–Teller (BET) or Guggenheim–Anderson–DeBoer (GAB) sorption isotherm models.

The BET model is described by the equation:

$$\frac{A_w}{(1-A_w)m} = \frac{1}{m_m K'} + \left[\frac{K'-1}{m_m K}\right] A_w \quad (1)$$

where K' is a constant, and mm is the BET monolayer value.

The GAB isotherm model is described by the equation:

$$\frac{m}{m_m} = \frac{CKA_w}{(1-KA_w)(1-KA_w+CKA_w)} \quad (2)$$

where K and C are constants, and m_m is the GAB monolayer value.

2.12. Mechanical properties

The stress-stain curves of the ESF were measured by the TA-XT Plus C texture analyzer (Stable Micro Systems, UK) and the elastic modulus, elongation at break, and tensile strength were obtained. All ESF were cut into rectangular strips (1 cm × 5 cm). The stretching speed was set at 0.5 mm/s with a 5 kg load cell. At least five tests were performed for each ESF.

2.13. Evaluation of antibacterial activity

The antibacterial activity of ESF was evaluated using the bacterial colony-counting method (Cai et al., 2021). Two typical food-borne pathogenic bacteria (Gram-negative bacteria *Escherichia coli* and Gram-positive bacteria *Staphylococcus aureus*) were used in this study. The ESF were sterilized and immersed in tubes containing 100 μL bacterial suspension (~10^7 CFU/mL) and 10 mL nutrient broth. All the tubes were shaken at 37 °C for 14 h. The growth inhibition rates (GIR) were calculated by the serial dilution plate counting process shown in Eq. (3).

$$GIR\,(\%) = \frac{initial\ colony\ amount\ -\ survival\ colony\ amount}{initial\ colony\ amount} \times 100 \quad (3)$$

2.14. Encapsulation and loading efficiency of EGCG

EGCG (50 mg) was addition to mixed PUL/EGCG and SAFs/PUL/EGCG electrospun solution (10 mL) respectively, and electrospun after stirring for half an hour without light irradiation. The EGCG loading efficiency of PUL/EGCG and SAFs/PUL/EGCG films was calculated using UV–vis spectroscopy. A fixed amount of ESF (80 mg) was immersed in phosphate buffer solution (pH 7.2) until complete dissolution. The amount of EGCG in these samples was obtained by measuring the UV absorbance value of the mixture solution. The detection wavelength was 278 nm, and the sample without EGCG was used as a control. The EGCG loading efficiency was calculated by the following equation Eq. (4).

$$Loading\ efficiency\,(\%) = \frac{released\ EGCG\ amount}{initial\ EGCG\ amount} \times 100 \quad (4)$$

2.15. Simulation of oral disintegration

The disintegration of the ESF of PUL/EGCG and SAFs/PUL/EGCG was measured using UV–vis spectroscopy. The simulated oral environment was configured according to the method of Minekus et al. (2014) with some modifications. 80 mg of each sample and 0.5 mL salivary α-amylase solution of 1500 U/mL were submerged in 100 mL of the simulated environment (pH 6.8). The mixed solution dissolved at 200 rpm for 10 min at room temperature. The amount of EGCG released in the simulated environment was quantified by UV–Vis spectroscopy by taking 10 mL of the release solution at a time.

Table 1
Viscosity, conductivity, and surface tension of PUL/SAFs in different proportion and SPI/PUL at a ratio of 4:6 (w/w).

Samples (w/w)	Viscosity (mPa·s)	Conductivity (mS/cm)	Surface tension (mN/m)
SAFs	2188.00^{d} ± 355.40	5.31^{a} ± 0.01	25.38^{e} ± 0.30
PUL	4568.33^{a} ± 107.97	0.19 ^{g} ± 0.05	50.33^{a} ± 0.53
SAFs/PUL 1:9	3031.67^{b} ± 125.13	2.73^{e} ± 0.09	33.90^{d} ± 0.41
SAFs/PUL 2:8	2215.00^{c} ± 197.93	3.03^{de} ± 0.09	35.29^{d} ± 0.31
SAFs/PUL 3:7	1318.33^{e} ± 132.51	3.27 ^{cd} ± 0.15	36.79 ^{cd} ± 0.11
SAFs/PUL 4:6	1188.33^{e} ± 121.07	3.35^{bc} ± 0.09	41.68^{c} ± 0.27
SAFs/PUL 5:5	1110.00^{e} ± 215.000	3.64^{b} ± 0.12	34.40^{d} ± 0.11
SPI/PUL 4:6	1033.33^{e} ± 179.19	3.29 ^{cd} ± 0.15	42.27^{bc} ± 0.06

$^{a–g}$Mean values in the same column followed by the same superscript letters are not significantly different ($p > 0.05$).

2.16. Statistical analysis

All experiments were performed as mean values ± standard deviation (SD) at least triplicates. Different batches of prepared electrospun films were used for each one replicate experiment. All data were evaluated using one-way analysis of variance (ANOVA) using SPSS 16.0 (SPSS Inc., Chicago, IL, USA) and the statistical differences were analyzed by Duncan's test ($p < 0.05$).

3. Results and discussions

3.1. Electrospun solution properties

The electrospun solution consists of a mixture of pullulan and SAFs, and its properties are affected by the conversion of SPI to SAFs. Therefore, the properties of the SAFs were first characterized. As shown in Fig. 1**A**, ThT fluorescence intensity variation is generally considered as an indicator of the presence of protein conversion to amyloid fibrils (Huyst et al., 2021). The successful preparation of SAFs is evident from the change in fluorescence intensity. The microstructure of SAFs were analyzed by AFM as shown in Fig. 1**B**. There are two types present in the prepared SAF: coexisting fibrils-long fibrils that are rigid "mature fibrils", and short-curved fibrils that are flexible "immature fibril" (Yamaguchi et al., 2004). The conversion rate of the soy protein to SAFs was determined to be 68.13 %.

Electrospun is a one-step electrohydrodynamic process with output being determined by the properties of the electrospun solution and process parameter settings. The fabricated SAFs were mixed with pullulan to form an electrospun solution, in which the conductivity, surface tension and viscosity played a key role in determining the morphology of ESF (Ramazani, Rostami, Raeisi, Tabibiazar, & Ghorbani, 2019). As shown in Table 1, the viscosity of electrospun solutions decreased significantly with an increase in the concentration of SAFs. The viscosity is a function of polymer concentration and molecular weight. Therefore, the decrease in viscosity of the electrospun solution may be due to the lower molecular weight of SAFs (<200 kDa) and the overall reduction in solution concentration following the addition of SAFs. Furthermore, the addition of SAFs significantly increases the conductivity of the solution. The increase in conductivity has been attributed to positively charged SAFs and is also related to protein content, charge density, amino acid

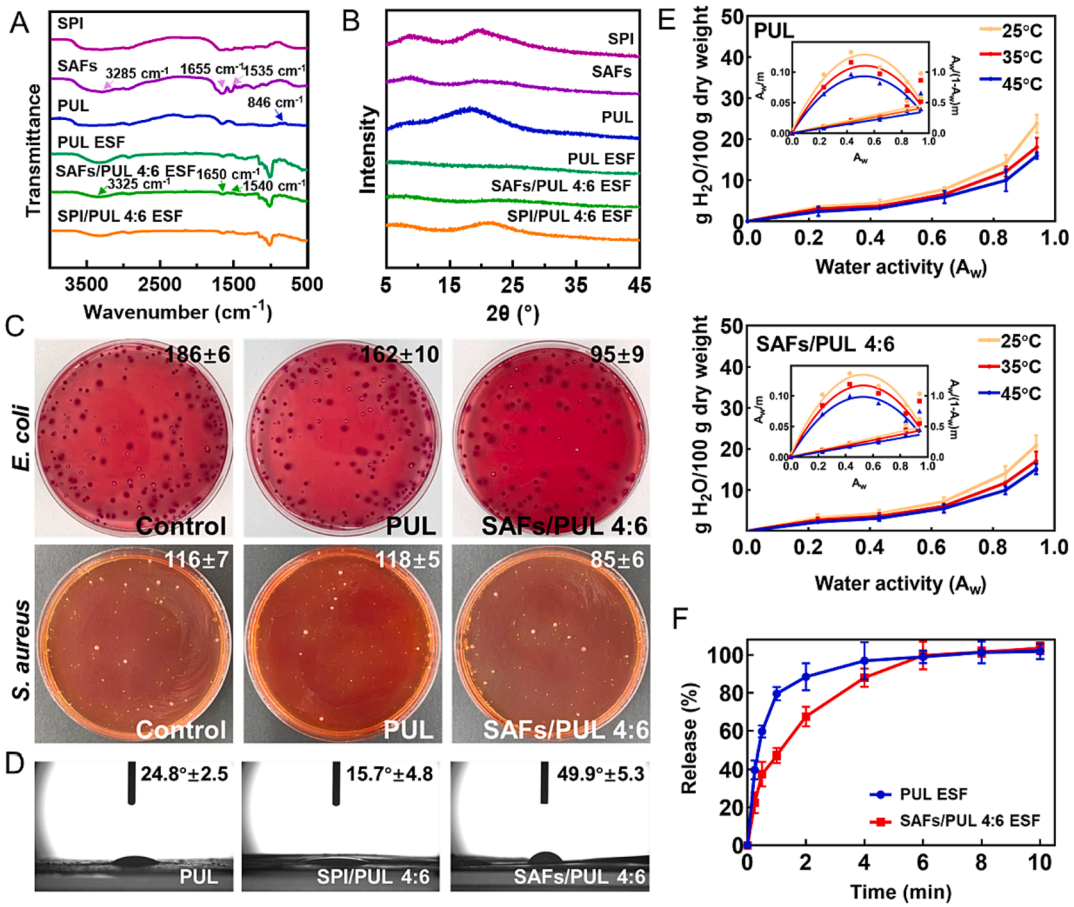

Fig. 2. (A) FTIR spectra of PUL, SAFs, SPI, PUL ESF, SAFs/PUL ESF and SPI/PUL ESF. (B) X-ray diffraction patterns of PUL, SAFs, SPI, PUL ESF, SAFs/PUL ESF and SPI/PUL ESF. (C) Bacterial colony-counting results of PUL ESF and SPI/PUL 4:6 ESF against *E. coli* and *S. aureus*. (D) Water contact angles of the PUL ESF, SPI/PUL 4:6 ESF and SAFs/PUL 4:6 ESF. (E) Water adsorption isotherms for PUL ESF and SAF/PUL 4:6 ESF (temperatures 25, 35 and 45 °C, water activity range 0.11–0.94). The corresponding GAB and BET plots are given in the insets. (F) Time dependent release profiles of PUL ESF and SAF/PUL 4:6 ESF.

composition and secondary structure (Kutzli, Gibis, Baier, & Weiss, 2019).

3.2. Morphology of electrospun films

To investigate the impact of SAFs on ESF, ESF samples were prepared at ratios ranging from 0:10 to 4:6 SAFs: PUL (higher ratio of SAFs solution cannot form fibers). The state of SAFs within ESF was investigated using fluorescence microscopy. As shown in Fig. 1**C**, SAFs were observed to be entangled within the ESF. We speculate that this may be due to SAFs being affected by voltage during the electrospun process and had difficulty maintaining its original state after exiting from the jet. The morphologies of the SAFs/PUL ESF were shown in Fig. 1**D.** The morphology of SAFs in ESF consistent with fluorescence microscopy is clearly observed in the Fig. 1**Dh**. In addition, as the addition of SAFs increased, the average diameter of electrospun fibers gradually decreased from 267.67 nm for PUL to 84.18 nm for SAFs/PUL 4:6. When the ratio of SAFs was up to SAFs/PUL 5:5, numerous spindle-like structure defects appeared along the electrospun fibers, accompanied by a higher frequency of holes on the electrospun film. In general, the spinnability of the electrospun solution is determined by its conductivity, while the conductivity and viscosity determine the formation of the final electrospun fiber. The spinnability of low viscosity solutions is generally controlled by surface tension, which is due to the repulsive electrostatic force generated by the electric field on the droplets flowing from the needle at the jet end. For a solution to be spinnable, it must overcome surface tension. In contrast, the cohesive nature of high viscosity solutions overcomes these conditions (Huang, Zhang, Kotaki, & Ramakrishna, 2003). In this study, an increase in the concentration of SAFs resulted in no significant change in the surface tension of the mixed solution, whereas the viscosity decreased significantly. Therefore, it was anticipated that the change in viscosity of the electrospun solution will determine the quality of the electrospun process. This conclusion is consistent with SEM images, where lower viscosity of the electrospun solution leads to a decrease in the average diameter of the electrospun fibers (Fig. 1**D**). As such, SPI/PUL 4:6 electrospun fibers were used as a comparison and there was no significant difference observed when compared with SAFs/PUL 4:6 electrospun fibers, which also indicated that the morphology of electrospun fibers was largely influenced by protein concentration and almost independent of protein state.

3.3. FTIR spectroscopy analysis

The FTIR spectrum of SAFs, SPI, pullulan and ESF structure are shown in Fig. 2**A**. FTIR was used to investigate potential interactions between the SAFs and pullulan. Pullulan is a linear homopolysaccharide composed of glucosyl units: maltotriose consisted of three glucose units connected by α-(1–4)-D-glucosidic bond, with consecutive maltotriose units connected by α-(1–6)-D-glucosidic bond (Shahriari-Khalaji et al., 2021). The strong absorption at 846 cm^{-1} is characteristic of a-D-glucopyranoside units. Other peaks at 753 cm^{-1} and 1015 cm^{-1} were attributed to the α-(1–6)-D-glucosidic bonds and α-(1–4)-D- glucosidic bonds, respectively (Prasad, Guru, Shivakumar, & Sheshappa Rai, 2012). Regarding the spectra of pullulan ESF within the 3500 and 3000

Table 2
Mechanical properties of PUL/SAFs in different proportion and SPI/PUL at a ratio of 4:6 (w/w).

Samples (w/w)	Elastic modulus (MPa)	Elongation at break (%)	Tensile strength (MPa)
PUL	$27.77^{b} \pm 1.51$	$11.12^{a} \pm 1.02$	$2.13^{a} \pm 0.62$
SAFs/PUL 1:9	$26.69^{b} \pm 9.33$	$8.83^{ab} \pm 1.67$	$1.39^{a} \pm 1.04$
SAFs/PUL 2:8	$43.61^{b} \pm 3.63$	$7.84^{abc} \pm 0.54$	$2.36^{a} \pm 2.15$
SAFs/PUL 3:7	$90.39^{a} \pm 2.21$	$4.32^{cd} \pm 0.99$	$2.82^{a} \pm 0.23$
SAFs/PUL 4:6	$91.28^{a} \pm 3.73$	$4.28^{cd} \pm 0.34$	$2.93^{a} \pm 0.73$
SPI/PUL 4:6	$82.64^{a} \pm 7.85$	$5.92^{bcd} \pm 0.27$	$3.41^{a} \pm 0.20$

[a–d]Mean values in the same column followed by the same superscript letters are not significantly different ($p > 0.05$).

cm^{-1} range, intensity-enhanced absorption peaks were observed, suggesting the formation of intermolecular hydrogen bonds between the pullulan chains during the electrospun process.

In the SAFs spectrum, the peak at 3285 cm^{-1} corresponded to the NH stretching band, and the absorption bands at 1651 cm^{-1} and 1538 cm^{-1} indicated the presence of amide I and amide II, respectively. Conformational transitions of SAFs from SPI were also investigated 1600–1700 cm^{-1} (amide I spectral region) of the FTIR spectra of SAFs and SPI. The results obtained from the analysis of the PeakFit (4.12, SeaSolve Software, Richmond, USA) revealed that the content of β-sheet structure in SAFs was 56.30 %, which was 3.4 % more than that of SPI (52.87 %). The increased content of the β-structure is an important sign of the formation of SAFs (Xu et al., 2022). From the spectra of SAFs/PUL 4:6 electrospun film, it was noticed that the amide I peak was shifted from 1655 cm^{-1} to 1650 cm^{-1} compared to SAFs. The amino peak of SAFs shifted from 1538 cm^{-1} to 1540 cm^{-1}. A shift in the bands of amide I vibration (mainly caused by C═O stretch) or II peaks vibration (combination of the CN stretch and the NH bending) indicates alterations in the secondary structures of SAFs, such as folding, unfolding and aggregation (Gounga, Xu, & Wang, 2010). Moreover, a shift in OH and NH stretching vibrations (from 3285 cm^{-1} to 3325 cm^{-1}) was also noticed. The shift of OH, NH, amide I and amide II reflect interactions due to hydrogen bonds between the hydroxyl groups of pullulan and the amino groups of SAFs.

3.4. X-ray diffraction characterization

The XRD patterns of SAFs, pullulan, SPI and ESF are shown in Fig. 2**B.** For SAFs, the two dominant peaks confirmed that the dominant secondary protein structure is β-sheet structure. Two diffraction peaks at $2\theta = 8.9°$ and $2\theta = 19.4°$ corresponded to the distance between stacked β-sheets and the spacing between β-strands, respectively (Riek & Eisenberg, 2016). In addition, SPI exhibited a strong characteristic reflection at $2\theta = 10.0°$ and $2\theta = 20.1°$, which was consistent with the work of Lan et al. (2020). A broad diffraction peak at $2\theta = 18.2°$ was also observed in the XRD pattern of pullulan, which suggests that pullulan had a typical non-crystalline structure. However, in the XRD patterns of the SAFs/PUL 4:6, SPI/PUL 4:6 ESF and PUL, the intensities of all observed characteristic peaks were weaker. This may be due to the formation of new hydrogen bonds between SAFs and PUL, and the creation of more amorphous structures during the electrospun process. In addition, the position of the amorphous peak of the ESF differed from the single samples (PUL, SPI, SAFs), which indicated potential physical interaction between the polysaccharide and protein (Kowalczyk, Skrzypek, Basiura-Cembala, Łupina, & Mężyńska, 2020).

3.5. Mechanical testing

The effect of the SAFs on the stress–strain properties of the SAFs/PUL ESF was studied by mechanical tensile tests. As shown in Table 2. The addition of SAFs significantly affected the elastic modulus and elongation at the break of the ESF, while the tensile strength was almost unaffected by SAFs. The incorporation of SAFs enhanced the elastic modulus, increasing it from 27.77 MPa for PUL electrospun film to 91.28 MPa for SAFs/PUL 4:6 electrospun film. Additionally, the incorporation of SAFs resulted in a decrease in elongation at break from 11.12 % for PUL electrospun film to 4.28 % for SAFs/PUL 4:6 electrospun film. These results evidenced a higher stiffness and lower flexibility of the SAFs/PUL ESF. A similar phenomenon was reported by Silva, Vilela, Almeida, Marrucho, and Freire (2018) in the preparation of nanocomposite films using lysozyme nanofibers and pullulan. In the study of Yang, Xie, Liu, Kong, and Wang (2020), ethyl cellulose was used to prepare electrospun film with enhanced mechanical properties by mixing pullulan. The elastic modulus and elongation at break of pullulan/ethyl cellulose nanofiber films were similar to that of SAFs/PUL ESF, but the SAFs/PUL ESF showed the enhanced tensile strength.

3.6. Antibacterial activity

The antimicrobial activity of ESF against *S. aureus* and *E. coli* was investigated by the bacterial colony-counting method. The growth inhibition rates of ESF against *E. coli* and *S. aureus* are shown in Fig. 2**C.** The experimental control was produced by inoculation of the *E. coli* and *S. aureus* in media in the absence of a sample. Results obtained indicated that PUL ESF did not show any inhibition effect, while the SAFs/PUL 4:6 ESF sample showed inhibition rates of 51.08 % against *E. coli* and 73.28 % against *S. aureus*. Results clearly showed that the SAFs confer antibacterial activity to the ESF. According to previous studies, the antibacterial functions of amyloid fibrils are achieved by disrupting the cell membrane (Cao & Mezzenga, 2019). Kummer et al. (2021) similarly reported that the increased hydrophobicity and positive charges of lysozyme amyloid fibrils enhanced the interaction with cell membranes. Therefore, we concluded that the hydrophobicity and the positive charge of SAFs may contribute to the antibacterial capacities of the ESF. Generally, in order to achieve the antibacterial activity of the prepared electrospun films, it is usually necessary to add supplementary antibacterial substances (Shahriari-Khalaji et al., 2021; Hsiung et al., 2022). However, in this study, the addition of SAFs alone not only improved the hydrophobicity and mechanical properties of the electrospun films but also conferred antibacterial activity to the electrospun films. This will help to reduce the preparation time and enhance the productivity of preparing electrospun films with multiple functionalities.

3.7. Water sorption behavior

The water contact angle (WCA) was measured to determine the sensitivity of the ESF to water. Higher WCA values indicate increased hydrophobicity, which suggests an ability to repel water. Furthermore, high hydrophobicity is advantageous for preserving food products, especially in humid environments (Suresh, Puspharaj, Natarajan, & Subramani, 2022). As shown in Fig. 2**D**, the WCA of the PUL electrospun film was 24.8°, indicating high hydrophilicity and high wettability. The addition of SPI in PUL ESF resulted in a decrease in the WCA value (from 24.8° to 15.7°). This may be due to the presence of hydroxyl, amino and carboxyl groups in SPI which increased the water adsorption capacity of the electrospun film. The WCA of SAFs/PUL electrospun film was 49.9°, which indicated greater hydrophobicity. This is likely due to the hydrophobicity of SAFs, which increased the hydrophobicity of SAFs/PUL ESF. To gain a better understanding of the water absorption characteristics, adsorption isotherms were performed.

The moisture sorption data of PUL and SAFs/PUL 4:6 ESF were obtained at 25, 35 and 45 °C are presented in Fig. 2**E.** The sorption isotherms obtained were sigmoidal, indicating that ESF is a material rich in hydrophilic components (Witczak, Stępień, Zięba, Gumul, & Witczak, 2020). The results demonstrate that an increase in A_w causes a slow

Table 3
Estimates of the BET and GAB parameters derived from moisture adsorption data for SAFs/PUL 4:6 and PUL electrospun films at three different temperatures (25, 35 and 45 °C).

Temperature	Electrospun films	GAB (A_w = 0.11–0.94)				BET (A_w = 0.11–0.64)		
		m_m (g H_2O per 100 g dry weight)	K	C	R^2	m_m (g H_2O per 100 g dry weight)	K'	R^2
25 °C	PUL	2.84	0.95	258.8	0.98	2.74	152.08	0.99
25 °C	SAF/PUL 4:6	2.71	0.94	165.3	0.98	2.57	162.21	0.99
35 °C	PUL	2.43	0.94	251.7	0.97	2.30	180.88	0.99
35 °C	SAF/PUL 4:6	2.29	0.94	147.9	0.98	2.17	135.50	0.99
45 °C	PUL	2.09	0.94	104.5	0.96	2.06	50.60	0.99
45 °C	SAF/PUL 4:6	2.00	0.94	99.7	0.97	1.94	59.32	0.99

increase in the equilibrium moisture content of all ESF. The isotherm shifted downward from 25 to 45 °C. The results showed that the water adsorption capacity was temperature dependent at constant A_w. The increase in temperature has a distinct impact on the mobility of water molecules and decreased the water adsorption capacity. The activation of water molecules due to an increase in temperature increased the mutual distance among water molecules and decreased the intermolecular attraction (mainly H-bonds) (McMinn & Magee, 2003). Furthermore, the moisture content of SAFs/PUL 4:6 ESF decreased compared to PUL ESF due to the presence of SAFs with higher hydrophobicity.

The monolayer value (m_m) is an adequate moisture content for many aspects of food stability, especially for foods with low or intermedium moisture content (Majd, Kordzadeh-Kermani, Ghalandari, Askari, & Sillanpää, 2021). Therefore, the water adsorption data of PUL and SAFs/PUL 4:6 ESF were fitted to the GAB and BET models to estimate monolayer values (Table 3). The three-parameter GAB isotherm model is widely recognized as a refinement and extension of the BET model by considering the properties of the water absorption in the multilayer regions and the heat of adsorption (Majd et al., 2021). In this study, the GAB isotherm describes the adsorption data for all temperatures and the entire relative humidity range, while the BET isotherm was suitable for water activity less than 0.64. The calculated monolayer values fell in a range of 2.06–2.84 and 1.94–2.71 g H_2O/100 g dry weight for PUL and SAFs/PUL 4:6 ESF, respectively. This result depended mainly on the storage temperature, and different adsorption models will also obtain different results. The SAFs/PUL 4:6 ESF showed lower monolayer values, which is consistent with the WCA results. This may be due to the fact that SAFs contained a higher number of exposed hydrophobic groups, reducing the water absorption capacity of SAFs/PUL 4:6. In addition, the monolayer values decreased with increasing storage temperature, which is the same as the majority of food materials (Drosou et al., 2018). The K values were between 0.94 and 0.95 and the C values between 99.7 and 258.8. This indicated that the difference between the estimated monolayer values and the true monolayer value is within ± 15.5 %. Previous studies reported that when C and K values fall within the intervals $5.67 \leq C \leq \infty$, $0.24 \leq K \leq 1$ in the GAB model, which indicated that the difference in simulation results was not more than ± 15.5 % (Kristo & Biliaderis, 2006). In summary, the addition of SAFs effectively reduces the moisture content in the ESF, which will help to enhance the stability and storage time of the ESF.

3.8. Simulation of oral disintegration

The loading efficiency of ESF was determined by dissolving samples in PBS. It was found that the pullulan ESF and the SAFs/PUL 4:6 ESF exhibited loading efficiencies of 98.7 ± 0.7 % and 99.1 ± 0.8 %, respectively. The results indicated that there was almost no loss of EGCG during sample preparation or the electrospun process. Similar results have been reported by Hsiung et al. (2022), who prepared nanofibers of pullulan/tetracycline-cyclodextrin inclusion complexes.

The time dependencies in simulated oral release profiles of PUL and SAFs/PUL 4:6 electrospun film have been summarized in Fig. 2**F**. The PUL electrospun film released 59.7 % of EGCG in just 30 s, reaching the maximum release percentage of 99.08 % within four minutes. On the other hand, SAFs/PUL 4:6 electrospun film released only 37.8 % of EGCG in 30 s and reached the maximum release percentage of 99.78 % within six minutes. A steady state profile was viewed for both samples over up to 10 min. This finding indicates that ESF released almost all the EGCG into the dissolution medium and the initial fast release stage occurred in the first six minutes. The rate of EGCG release from SAFs/PUL 4:6 ESF was slower than PUL ESF at the initial stage. Based on the water contact angle and water adsorption isotherm, it is known that the addition of SAFs resulted in the ESF being less hydrophilic and less hygroscopic such that the release rate of SAF/PUL 4:6 ESF was slower than that of PUL ESF. This release manner allowed for a slow and sustained release of EGCG in the oral cavity, which may be more beneficial for the absorption of EGCG, resulting in the prepared SAFs/PUL ESF having the potential for oral drug delivery, and for ESF doped with SAFs to provide a slower initial release and a relatively controlled release of encapsulated EGCG compared to PUL ESF.

4. Conclusions

In this study, the composite ESF of soy protein amyloid fibrils and pullulan were successfully prepared. The scanning electron microscopy and fluorescence microscopy results showed that the soy protein amyloid fibrils were entangled in the ESF. The composite films increased the mechanical strength by 3 times through intermolecular chain hydrogen bonding interactions compared to pullulan film without protein fibrils. In addition, the composite films prepared by protein fibrils and pullulan, displayed antimicrobial activities, stronger hydrophobic properties, and lower monolayer water values compared to films prepared by SPI and pullulan. These properties are essential for the application and storage of ESF. Moreover, the composite films encapsulated with EGCG were effectively released in a simulated oral disintegration, indicating that the composite film has the potential to be used as an oral rapid release film.

CRediT authorship contribution statement

Yabo Dong: Conceptualization, Methodology, Software, Writing – original draft. **Tian Lan:** Conceptualization, Methodology, Software, Writing – original draft. **Luying Wang:** Methodology. **Xing Wang:** Methodology. **Zejian Xu:** Methodology. **Lianzhou Jiang:** Visualization, Investigation. **Yan Zhang:** Visualization, Investigation. **Xiaonan Sui:** Supervision, Writing – review & editing.

Declaration of Competing Interest

The authors declare that they have no known competing financial interests or personal relationships that could have appeared to influence the work reported in this paper.

Data availability

Data will be made available on request.

Acknowledgement

We gratefully acknowledge the financial support received from the National Natural Science Foundation of China (32022068 and 32230082).

References

Akkermans, C., Van der Goot, A., Venema, P., Gruppen, H., Vereijken, J., Van der Linden, E., & Boom, R. (2007). Micrometer-sized fibrillar protein aggregates from soy glycinin and soy protein isolate. *Journal of Agricultural and Food Chemistry, 55* (24), 9877–9882. https://doi.org/10.1021/jf0718897

Cai, X., Tian, J., Zhu, J., Chen, J., Li, L., Yang, C., … Chen, D. (2021). Photodynamic and photothermal co-driven CO-enhanced multi-mode synergistic antibacterial nanoplatform to effectively fight against biofilm infections. *Chemical Engineering Journal, 426*, Article 131919. https://doi.org/10.1016/j.cej.2021.131919

Cao, Y., & Mezzenga, R. (2019). Food protein amyloid fibrils: Origin, structure, formation, characterization, applications and health implications. *Advances in Colloid and Interface Science, 269*, 334–356. https://doi.org/10.1016/j.cis.2019.05.002

Dong, Y., Lan, T., Huang, G., Jiang, L., Zhang, Y., & Sui, X. (2021). Development and characterization of nanoparticles formed by soy peptide aggregate and epigallocatechin-3-gallate as an emulsion stabilizer. *LWT, 152*, Article 112385. https://doi.org/10.1016/j.lwt.2021.112385

Dong, Y., Lan, T., Wang, X., Zhang, Y., Jiang, L., & Sui, X. (2020). Preparation and characterization of soy protein microspheres using amorphous calcium carbonate cores. *Food Hydrocolloids, 107*, Article 105953. https://doi.org/10.1016/j.foodhyd.2020.105953

Dos Santos, D. M., Correa, D. S., Medeiros, E. S., Oliveira, J. E., & Mattoso, L. H. (2020). Advances in functional polymer nanofibers: From spinning fabrication techniques to recent biomedical applications. *ACS Applied Materials & Interfaces, 12*(41), 45673–45701. https://doi.org/10.1021/acsami.0c12410

Drosou, C., Krokida, M., & Biliaderis, C. G. (2018). Composite pullulan-whey protein nanofibers made by electrospinning: Impact of process parameters on fiber morphology and physical properties. *Food Hydrocolloids, 77*, 726–735. https://doi.org/10.1016/j.foodhyd.2017.11.014

Drosou, C., Krokida, M., & Biliaderis, C. G. (2022). Encapsulation of β-carotene into food-grade nanofibers via coaxial electrospinning of hydrocolloids: Enhancement of oxidative stability and photoprotection. *Food Hydrocolloids, 133*, Article 107949. https://doi.org/10.1016/j.foodhyd.2022.107949

Fabra, M., Talens, P., & Chiralt, A. (2010). Water sorption isotherms and phase transitions of sodium caseinate–lipid films as affected by lipid interactions. *Food Hydrocolloids, 24*(4), 384–391. https://doi.org/10.1016/j.foodhyd.2009.11.004

Gounga, M. E., Xu, S., & Wang, Z. (2010). Film forming mechanism and mechanical and thermal properties of whey protein isolate-based edible films as affected by protein concentration, glycerol ratio and pullulan content. *Journal of Food Biochemistry, 34* (3), 501–519. https://doi.org/10.1016/j.jfoodeng.2007.04.008

Hsiung, E., Celebioglu, A., Chowdhury, R., Kilic, M. E., Durgun, E., Altier, C., & Uyar, T. (2022). Antibacterial nanofibers of pullulan/tetracycline-cyclodextrin inclusion complexes for Fast-Disintegrating oral drug delivery. *Journal of Colloid and Interface Science, 610*, 321–333. https://doi.org/10.1016/j.jcis.2021.12.013

Huang, Z., Zhang, Y., Kotaki, M., & Ramakrishna, S. (2003). A review on polymer nanofibers by electrospinning and their applications in nanocomposites. *Composites Science and Technology, 63*(15), 2223–2253. https://doi.org/10.1016/S0266-3538(03)00178-7

Huyst, A. M., Deleu, L. J., Luyckx, T., Lambrecht, M. A., Van Camp, J., Delcour, J. A., & Van der Meeren, P. (2021). Influence of hydrophobic interfaces and shear on ovalbumin amyloid-like fibril formation in oil-in-water emulsions. *Food Hydrocolloids, 111*, Article 106327. https://doi.org/10.1016/j.foodhyd.2020.106327

Knowles, T. P., Oppenheim, T. W., Buell, A. K., Chirgadze, D. Y., & Welland, M. E. (2010). Nanostructured films from hierarchical self-assembly of amyloidogenic proteins. *Nature Nanotechnology, 5*(3), 204–207. https://doi.org/10.1038/nnano.2010.26

Kowalczyk, D., Skrzypek, T., Basiura-Cembala, M., Łupina, K., & Mężyńska, M. (2020). The effect of potassium sorbate on the physicochemical properties of edible films based on pullulan, gelatin and their blends. *Food Hydrocolloids, 105*, Article 105837. https://doi.org/10.1016/j.foodhyd.2020.105837

Kristo, E., & Biliaderis, C. G. (2006). Water sorption and thermo-mechanical properties of water/sorbitol-plasticized composite biopolymer films: Caseinate–pullulan bilayers and blends. *Food Hydrocolloids, 20*(7), 1057–1071. https://doi.org/10.1016/j.foodhyd.2005.11.008

Kummer, N., Wu, T., De France, K. J., Zuber, F., Ren, Q., Fischer, P., … Nyström, G. (2021). Self-Assembly pathways and antimicrobial properties of lysozyme in different aggregation states. *Biomacromolecules, 22*(10), 4327–4336. https://doi.org/10.1021/acs.biomac.1c00870

Kutzli, I., Gibis, M., Baier, S. K., & Weiss, J. (2019). Electrospinning of whey and soy protein mixed with maltodextrin–Influence of protein type and ratio on the production and morphology of fibers. *Food Hydrocolloids, 93*, 206–214. https://doi.org/10.1016/j.foodhyd.2019.02.028

Leng, X., Cheng, S., Wu, H., Nian, Y., Zeng, X., & Hu, B. (2022). High internal phase emulsions stabilized with Polyphenol-Amyloid fibril supramolecules for encapsulation and protection of lutein. *Journal of Agriculatural and Food Chemistry, 70*(7), 2328–2338. https://doi.org/10.1021/acs.jafc.1c04615

Majd, M. M., Kordzadeh-Kermani, V., Ghalandari, V., Askari, A., & Sillanpää, M. (2021). Adsorption isotherm models: A comprehensive and systematic review (2010–2020). *Science of The Total Environment, 812*, Article 151334. https://doi.org/10.1016/j.scitotenv.2021.151334

McMinn, W., & Magee, T. (2003). Thermodynamic properties of moisture sorption of potato. *Journal of Food Engineering, 60*(2), 157–165. https://doi.org/10.1016/S0260-8774(03)00036-0

Mehmood, S., Maqsood, M., Mahtab, N., Khan, M. I., Sahar, A., Zaib, S., & Gul, S. (2022). Epigallocatechin gallate: Phytochemistry, bioavailability, utilization challenges, and strategies. *Journal of Food Biochemistry, 46*, e14189.

Minekus, M., Alminger, M., Alvito, P., Ballance, S., Bohn, T., Bourlieu, C., … Dupont, D. (2014). A standardised static in vitro digestion method suitable for food–an international consensus. *Food & Function, 5*(6), 1113–1124. https://doi.org/10.1039/C3FO60702J

Niu, B., Zhan, L., Shao, P., Xiang, N., Sun, P., Chen, H., & Gao, H. (2020). Electrospinning of zein-ethyl cellulose hybrid nanofibers with improved water resistance for food preservation. *International Journal of Biological Macromolecules, 142*, 592–599. https://doi.org/10.1016/j.ijbiomac.2019.09.134

Peng, W., Min-Hua, Z., Robert, L., Kun, F., & Hong, W.u. (2017). Electrospinning: A novel nano-encapsulation approach for bioactive compounds. *Trends in Food Science & Technology, 70*, 56–58. https://doi.org/10.1016/j.tifs.2017.10.009

Peydayesh, M., & Mezzenga, R. (2021). Protein nanofibrils for next generation sustainable water purification. *Nature Communications, 12*(1), 1–17. https://doi.org/10.1038/s41467-021-23388-2

Prasad, P., Guru, G., Shivakumar, H., & Sheshappa Rai, K. (2012). Investigation on miscibility of sodium alginate/pullulan blends. *Journal of Polymers and the Environment, 20*(3), 887–893. https://doi.org/10.1007/s10924-012-0427-4

Ramazani, S., Rostami, M., Raeisi, M., Tabibiazar, M., & Ghorbani, M. (2019). Fabrication of food-grade nanofibers of whey protein Isolate-Guar gum using the electrospinning method. *Food Hydrocolloids, 90*, 99–104. https://doi.org/10.1016/j.foodhyd.2018.12.010

Riek, R., & Eisenberg, D. S. (2016). The activities of amyloids from a structural perspective. *Nature, 539*(7628), 227–235. https://doi.org/10.1038/nature20416

Shahriari-Khalaji, M., Hu, G., Chen, L., Cao, Z., Andreeva, T., Xiong, X., … Hong, F. (2021). Functionalization of aminoalkylsilane-grafted bacterial nanocellulose with ZnO-NPs-doped pullulan electrospun nanofibers for multifunctional wound dressing. *ACS Biomaterials Science & Engineering, 7*(8), 3933–3946. https://doi.org/10.1021/acsbiomaterials.1c00444

Silva, N. H., Vilela, C., Almeida, A., Marrucho, I. M., & Freire, C. S. (2018). Pullulan-based nanocomposite films for functional food packaging: Exploiting lysozyme nanofibers as antibacterial and antioxidant reinforcing additives. *Food Hydrocolloids, 77*, 921–930. https://doi.org/10.1016/j.foodhyd.2017.11.039

Suresh, S. N., Puspharaj, C., Natarajan, A., & Subramani, R. (2022). Gum acacia/pectin/pullulan-based edible film for food packaging application to improve the shelf-life of ivy gourd. *International Journal of Food Science & Technology, 57*(9), 5878–5886. https://doi.org/10.1111/ijfs.15909

Tang, C. (2019). Nanostructured soy proteins: Fabrication and applications as delivery systems for bioactives (a review). *Food Hydrocolloids, 91*, 92–116. https://doi.org/10.1016/j.foodhyd.2019.01.012

Witczak, T., Stępień, A., Zięba, T., Gumul, D., & Witczak, M. (2020). The influence of extrusion process with a minimal addition of corn meal on selected properties of fruit pomaces. *Journal of Food Process Engineering, 43*(4), e13382.

Xu, C., Ma, J., Wang, W., Liu, Z., Gu, L., Qian, S., … Jiang, Z. (2022). Preparation of pectin-based nanofibers encapsulating Lactobacillus rhamnosus 1.0320 by electrospinning. *Food Hydrocolloids, 124*, Article 107216. https://doi.org/10.1016/j.foodhyd.2021.107216

Xu, Z., Hao, N., Li, L., Zhang, Y., Yu, L., Jiang, L., & Sui, X. (2019). Valorization of soy whey wastewater: How epigallocatechin-3-gallate regulates protein precipitation. *ACS Sustainable Chemistry & Engineering, 7*(18), 15504–15513. https://doi.org/10.1021/acssuschemeng.9b03208

Xu, Z., Shan, G., Hao, N., Li, L., Lan, T., Dong, Y., … Jiang, L. (2022). Structure remodeling of soy protein-derived amyloid fibrils mediated by epigallocatechin-3-gallate. *Biomaterials, 283*, Article 121455. https://doi.org/10.1016/j.biomaterials.2022.121455

Yamaguchi, K.-I., Katou, H., Hoshino, M., Hasegawa, K., Naiki, H., & Goto, Y. J. (2004). Core and heterogeneity of β_2-microglobulin amyloid fibrils as revealed by H/D exchange. *Journal of Molecular Biology, 338*(3), 559–571. https://doi.org/10.1016/j.jmb.2004.02.067

Yang, Y., Xie, B., Liu, Q., Kong, B., & Wang, H. (2020). Fabrication and characterization of a novel polysaccharide based composite nanofiber films with tunable physical properties. *Carbohydrate Polymers, 236*, Article 116054. https://doi.org/10.1016/j.carbpol.2020.116054

Yue, J., Shu, M., Yao, X., Chen, X., Li, D., Yang, D., … Jiang, F. (2022). Fibrillar assembly of whey protein isolate and gum Arabic as iron carrier for food fortification. *Food Hydrocolloids, 128*, Article 107608. https://doi.org/10.1016/j.foodhyd.2022.107608